A practical method to remove *a priori* information from lidar Optimal Estimation Method Retrieval

Ali Jalali[1], Shannon Hicks-Jalali[1], Robert J. Sica[1,2], Alexander Haefele[2,1], and Thomas von Clarmann[3]

[1]Department of Physics and Astronomy, The University of Western Ontario, London, Canada

[2]Federal Office of Meteorology and Climatology, MeteoSwiss, Payerne, Switzerland

[3]Forschungszentrum Karlsruhe, Institut fu?r Meteorologie und Klimaforschung, Karlsruhe, Germany

Correspondence to: sica@uwo.ca

Abstract. OEM lidar retrievals are set up per predefined fine grids which usually the number of vertical levels in the fine grid is more than pieces of independent information (degree of freedom) in the measurements. A retrieved lidar profile in this condition contains some information from *a priori* which might affect the results in the top part of profiles in the cases of OEM lidar Rayleigh and water vapour retrievals. *A priori* removal from the retrieved profiles in the regions of prevailing *a priori* effect would help to analyses the results more accurately. One solution could be transforming an OEM retrieved profile from a fine grid to a coarser grid such that the averaging kernel be close enough to unity. In this case, setting the *a priori* trem in the OEM retrieval equation leads the to minimize the effect of *a priori* in the coarse grid retrieval. The Rayleigh channel temperature retrieval from the PCL and RALMO lidar as well as RALMO water vapour retrieval are used to demonstrate the presented approach or *a priori* removal.

1 introduction

-history of OEM - why do we need oem - what is the effect of apriori on retrieval - PCL and RALMO

2 Methodology

- satelite usage (von Clarmann paper) - manipulation of equation (R=0) - practical application and method (steps)

3 Results

3.1 PCL

AKM uncertainty budget temp retrieval

3.2 Ralmo

T WV

3.3 T diff US and CIRA

4 Discussion

A priori has an effect that is less than stat. unce., but can be removed at the cost of high uncertainty.

5 Introduction

Rodgers (2011) introduced an Optima Estimation Method (OEM) which is based on information theory, to use in atmospheric remote sensing area. Recently, Sica and Haefele (2015) and Sica and Haefele (2016) applied the OEM technique in the lidar research field to retrieve the atmospheric temperature and water vapour from Rayleigh and water vapour lidar channels, respectively. In the case of lidar Rayleigh and water vapour channels, the amount of information in the measurements vary based on the atmospheric states like temperature and water vapour concentration. The OEM retrieval results comprises from lidar measurements and *apriori* information.*a priori* is a knowledge that we have about the atmospheric state before making the measurements. The contribution of the *a priori* is different at different altitudes in the retrieved states. The OEM provides a diagnostic tools like averaging kernel which can be used to show the amount of information determined by lidar measurements and the portion carry by *a priori* information at each altitude. Lidars take advantage of high temporal and spatial resolution and the OEM retrieval grid, which is fairly fine. The independent pieces of information in the retrieval decreases by altitude due to the decreasing signal to noise ratio. The majority of the retrieval in the lower parts of the retrieved profiles even with fine retrieval grid are coming from lidar measurements but in the higher altitudes, *a priori* contribution to the retrieval increases. This can be an issue when various *a prioris* are used and the results will be questionable in the areas that *a priori* has higher contribution in the retrieval. As, it is difficult to distinguish if retrieved profiles structure is due to the *a priori* constraint or the atmospheric state. Several solutions have been suggested by Vincent et al. (2015), Ceccherini et al. (2009), von Clarmann and Grabowski (2007) and Joiner and Silva (1998). The idea to minimize the effect of *a priori* was based on transforming a regularized retrieval to a maximum likelihood from the fine grid to a coarser grid. The presented work trying to apply von Clarmann and Grabowski (2007) approach for grid transformation to the retrieved lidar profiles of temperature and water vapour. The transformation is applied in a way that each grid point carries one degree of freedom. Then, the retrieved profiles are calculated in the coarse grid by rerunning the OEM in a way that the effect of *a priori* constraint is minimized.

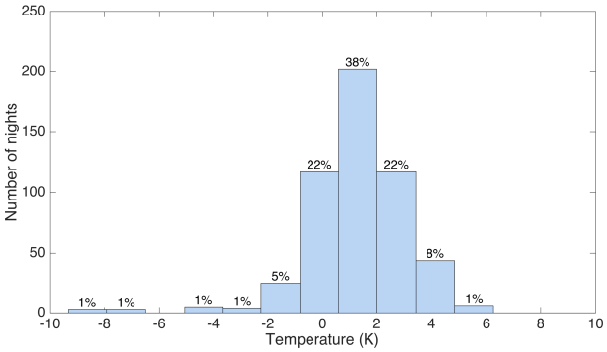

Figure 1. Distribution of the differences in temperatures retrieved at the 0.9 cutoff using two *a priori* temperature profiles - US Standard Atmosphere and CIRA-86.

6 OEM theoretical background

Optimal Estimation Method (OEM) is a type of inverse modelling based on Bayesian statistics. The OEM uses Gaussian probability density functions (PDF) in order to maximize the probability of the retrieved state based on the value of the measurements and choice of *a priori*. In other word, the OEM minimizes a cost function, comprised from measurements and *a priori* components. The general OEM forward model equation can be written as:

$$\mathbf{y} = \mathbf{F}(\mathbf{x}, \mathbf{b}) + \epsilon, \tag{1}$$

where **y** is the measurement vector which includes measurement noise (ϵ), **F** is the forward model, **x** stands for the state vector and **b** stands for all model parameters which have impact on the measurements.

The possible values of measurements are distributed by the PDFs. The OEM approach finds the state vector which most likely is consistent with the measurements and a priori information.

If the forward model is sufficiently linear or moderately nonlinear, the Eq. 1 around $\mathbf{x_a}$ can be written as:

$$\mathbf{y} - \mathbf{F}(\mathbf{x_a}) = \mathbf{K}(\mathbf{x} - \mathbf{x_a}) + \epsilon. \tag{2}$$

K referred to the Jacobian matrix. The solution of Eq. 2 is given by

$$\hat{\mathbf{x}} = \mathbf{x_a} + (\mathbf{K}^T {\boldsymbol{S_\epsilon}}^{-1}\mathbf{K} + {\boldsymbol{S_a}}^{-1})^{-1}\mathbf{K}^T {\boldsymbol{S_\epsilon}}^{-1}(\mathbf{y} - \mathbf{F}(\mathbf{x_a})) = \mathbf{x_a} + \mathbf{G}(\mathbf{y} - \mathbf{F}(\mathbf{x_a})), \tag{3}$$

where $\mathbf{G}$ is the gain matrix, $\mathbf{S}_\epsilon$ is the covariance matrix of the error measurements and $\mathbf{x_a}$ is *a priori* with its covariance, $\mathbf{S_a}$. The gain matrix describes the sensitivity of the retrieval to the observations:

$$\mathbf{G} = \frac{\partial \hat{\mathbf{x}}}{\partial \mathbf{y}} = (\mathbf{K}^T \boldsymbol{S_\epsilon}^{-1} \mathbf{K} + \boldsymbol{S_a}^{-1})^{-1} \mathbf{K}^T \boldsymbol{S_\epsilon}^{-1}. \tag{4}$$

A diagnostic tool that provides some information about the retrieval is averaging kernel matrices ($\mathbf{A}$) which represents the sensitivity of the retrieved state to the true state. At each retrieval grid point (level or altitude), the averaging kernel gives the maximum sensitivity. As the PDFs of retrieval state follows Gaussian distribution, full width at half maximum of the averaging kernel at each altitude represents the vertical resolution. Eq. 3 can be rewritten based on the averaging kernel,

$$\hat{\mathbf{x}} = (\mathbf{I_n} - \mathbf{A})\mathbf{x_a} + \mathbf{A}\mathbf{x} + \mathbf{G}\epsilon, \tag{5}$$

where $\mathbf{I_n}$ is the identity matrix of the size of $\mathbf{A}$. Eq. 5 clearly shows that if the $\mathbf{A}$ equals 1 at each altitude, the retrieval is just coming from measurements and there is not any information from *a priori*. Whatever, $\mathbf{A}$ is smaller than 1, the contribution of *a priori* increase in the retrieved state. Another useful application of averaging kernel is the trace of the $\mathbf{A}$ which represents the degree of freedom of signal,

$$dgf = Tr(\mathbf{A}). \tag{6}$$

In a perfect condition that the contribution of the *a priori* is zero in all levels, the dgf equals to the number of levels (state parameters).

7 Methodology

In general, soft constraints are the constraints that are needed to be determined approximately rather than exactly in a relation and it has some uncertainties in a relations between variables. The opposite of the soft constraint is hard that should be defined rigorously and accurately and the relation between the state variables are known exactly. The inverse of *a priori* covariance matrix ($\mathbf{S_a^{-1}}$) in Eq. 3 is known as regularization term. The regularization term is a soft constraint in Eq. 3. If $\mathbf{S_a^{-1}}$ set to zero, the Optimal Estimation becomes the unconstrained least squares solution (von Clarmann and Grabowski, 2007) (hard constraint). von Clarmann and Grabowski (2007) proposed an approach to remove the effect of *a priori* from the OEM retrieval based on information centered grid approach. Each level of the retrieval vertical grid points in the information centered grid contains one degree of freedom and therefore, the number of degree of freedom of signal is same as the number of the retrieval levels. In this condition, the effect of *a priori* is removed from the retrieval. von Clarmann and Grabowski (2007) have presented a method to reregularize the retrieval on a coarser grid after performing the OEM retrieval on a fine grid. The method used a representation to transform the retrieved data from the fine grid to a coarser grid in a way that the averaging kernel matrix in the coarse grid equals one at each vertical grid point. In this cased the effect of *a priori* is minimal. von Clarmann and Grabowski (2007)

presented two approaches, staircase representation and triangular representation in order to transform the retrieval from fine to coarse grid. The cumulative trace of $\mathbf{A}$ shows the the total degree of freedom of the retrieval. In these representations, the cumulative trace of $\mathbf{A}$ as a function of altitude is calculated and it then interpolated to the equal numbers of spaces (coarse grid) based on the centered information approach. As each space contains one degree of freedom, the spaces distributed irregularly. The staircase representation is not a realistic representation for the atmosphere (von Clarmann and Grabowski, 2007), therefore we use the triangular representation in this research work. In the triangular representation the highest and lowest level of coarse grid is considered same as the fine grid and the rest of the grid points are distributed in a manner that each elements of $\mathbf{A}$ at each level is close to one. The method that followed in this research is after running the OEM for a first time, the triangular representation applied to the fine retrieval grid to find the coarse grid. The $\mathbf{A}$ in this coarse grid equals one. Then, the coarse grid is chosen as a new retrieval grid for the OEM and the $\mathbf{S_a^{-1}}$ set to zero with choosing a large uncertainty for the *a priori* covariance matrix. The OEM is run again using the new coarse retrieval grid and the effect of the *a priori* is minimal due to $\mathbf{S_a^{-1} = 0}$.

8 Application of Technique

Our goal apply an information-centered approach using von Clarmann and Grabowski (2007)'s triangular representation to the lidar OEM retrievals in order to remove the effect of *a priori* from the retrievals. This approach is applied to the PCL and RALMO Rayleigh temperature retrievals and the RALMO water vapour daytime and nighttime retrievals. This method is also applicable to other lidar retrievals such as Ozone and Raman temperature, but were not explored in this study. First we will discuss the results from the triangular representation and the creation of the "coarse grid" and how it is used as the new retrieval grid. Then we will discuss its effect on the retrieval, vertical resolution, uncertainty budgets, and averaging kernel.

8.1 Purple Crow Lidar Rayleigh temperature *a priori* removal

We picked a sample night, May 25 2015, from the Rayleigh temperature climatology to illustrate the *a priori* removal procedure. The original OEM retrieval fine grid was 1024 m, and the *a priori* temperatures were taken from CIRA-86. The details regarding the OEM retrieval are discussed in Jalali et al. (2018). Figure 2 shows the estimate of the number of points which are used to create the coarse grid from the fine grid. The final altitudes which are used in the coarse grid are shown in Figure 3. As the sensitivity of the averaging kernel decreases the number of points used in the coarse grid from the fine grid increases. The distance between the second to last and the last point contains only 1 degree of freedom.

The averaging kernels for the fine grid and coarse grid retrievals are shown in Fig. 4. In this figure the red line is the measurement response, or the estimate of the averaging kernel's sensitivity to the measurements. The height at which the measurement response equals 0.9 was chosen as a "cutoff" height in Jalali et al. (2018). After applying the *a priori* removal, the averaging kernel on the coarse grid is equal to 1 at each point. This shows that at the coarse grid points, the averaging kernel is completely sensitive to the measurements and therefore there is no *a priori* contribution.

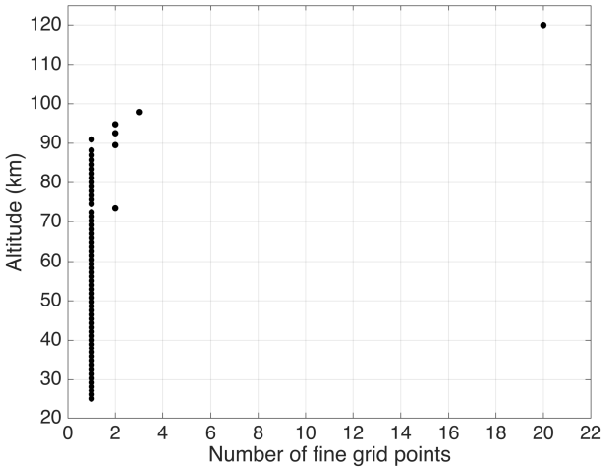

Figure 2. The number of fine grid points used to calculate the coarse grid.

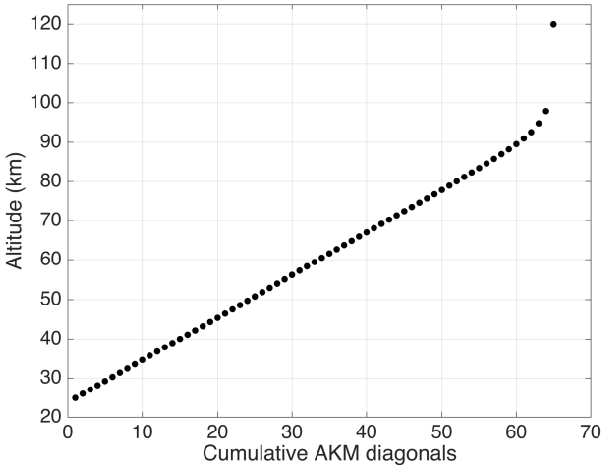

Figure 3. The coarse grid altitude.

One consequence of applying this method is that the uncertainties in the retrieval (Fig. 5) increase where the coarse grid is not equal to the fine grid. The most sensitive uncertainty parameter is the statistical uncertainty, which changes from 13 K to 20 K at 98 km. The rest of the systematic uncertainties are not affected, with the exception of the uncertainty due to the seed pressure. The uncertainty due to seed pressure decreases BECAUSE OF WHAT???

The vertical resolution for both grids is equal up 85 km, but as the coarse grid incorporates more points from the fine grid, the vertical resolution increases rapidly (Fig. 6). The last altitude in the vertical resolution is smaller than the previous altitude's due to the averaging kernel being incomplete CHECK THIS!!!!

Fig. 7 shows the OEM temperature retrieval on with and without the *a priori*. The two retrievals are identical up to 88 km. After 88 km the coarse grid retrieval differs from the fine grid retrieval and shows temperature layers similar to the matching

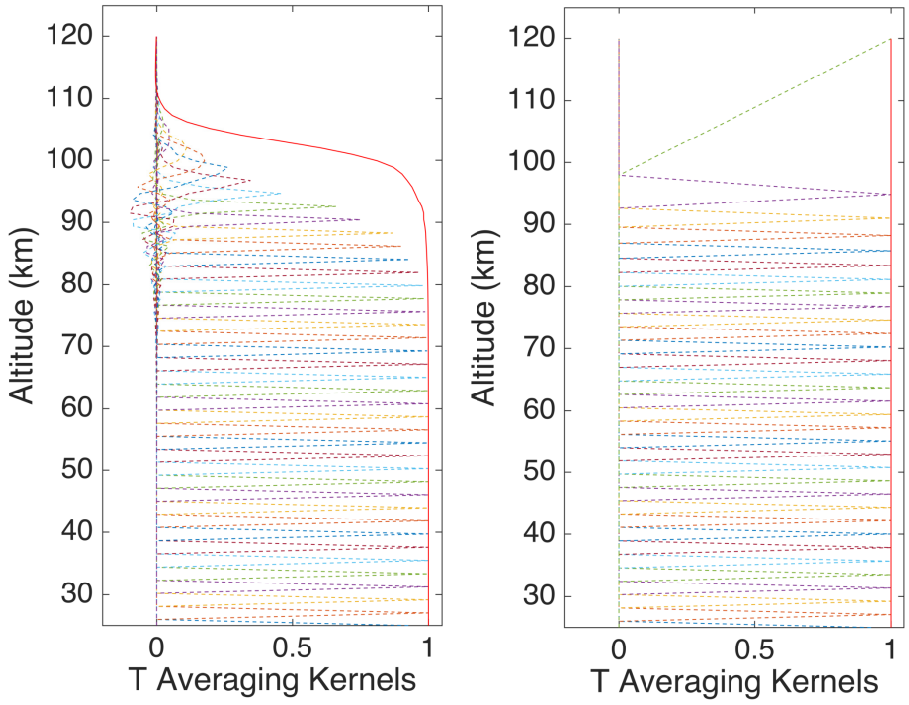

Figure 4. The averaging kernel matrix on the fine grid (left) and on the coarse grid (right).

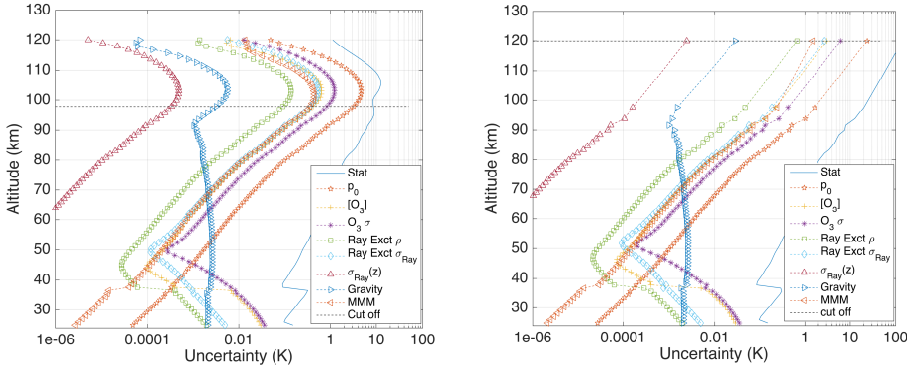

Figure 5. Total uncertainty budget on the fine (left) and coarse (right) grid.

SABER profile, however, the features detected by SABER are shifted roughly 5 km higher in altitude than what the lidar detects. Above 110 km the fine grid retrieval falls back on the *a priori*. To determine the validity of this method, we compared the temperature retrievals using two different *a priori*, the CIRA-86 and the US Standard Atmosphere in Fig. 8. The difference between the two temperatures on the fine grid retrieval is shown by the black curve and was 2 K at the 0.9 line and is well within the statistical uncertainty. However, the difference increases rapidly above that height. The same temperature difference after the *a priori* is removed is shown in red and is zero for all altitudes.

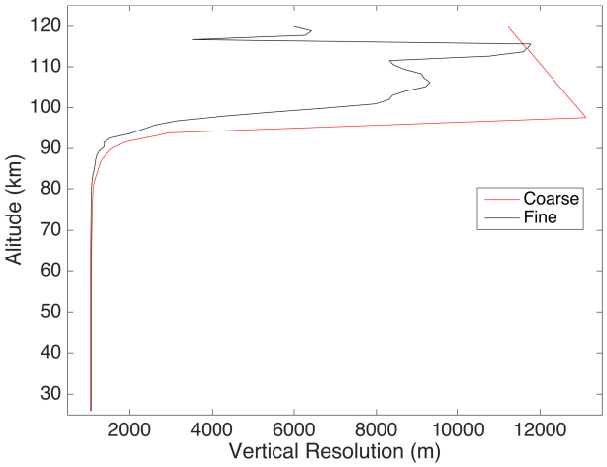

Figure 6. The vertical resolution.

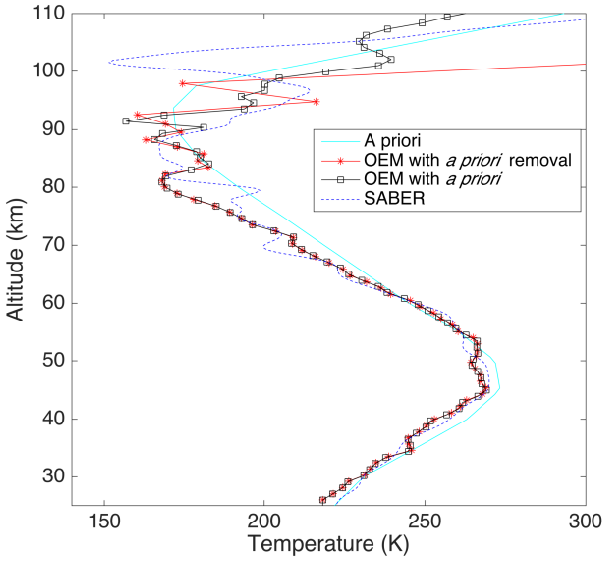

Figure 7. The retrieved temperature.

8.2 RALMO Rayleigh temperature *a priori* removal

RALMO was not built to measure the Rayleigh channel in order to retrieve the temperature above 30 km, where the effect of aerosols can be ignored. The main purpose of this channel is to measure the aerosols backscatter ratio, which can be used in water vapour and Raman temperature retrievals. Therefore, the Rayleigh temperature retrieval has not evaluated and this is first time we try to retrieve the temperature from RALMO Rayleigh measurements. However, because the Rayleigh signal for this channel is very weak above 30 km (Fig. 9), we decided to retrieve the Rayleigh temperature above 20 km. Typical return

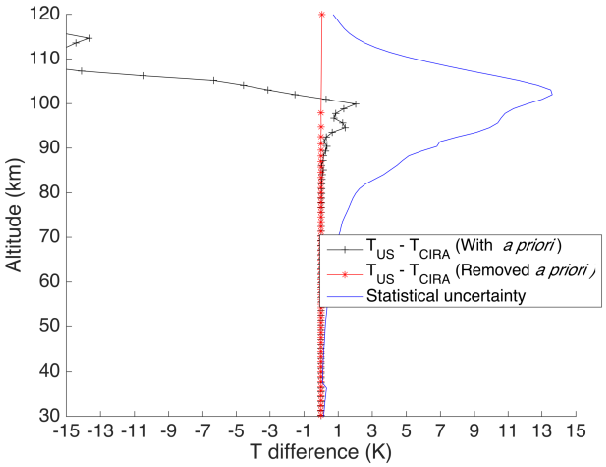

Figure 8. Temperature difference between the OEM retrieved temperature profiles using US Standard Atmosphere and CIRA-86 as the*a priori*.

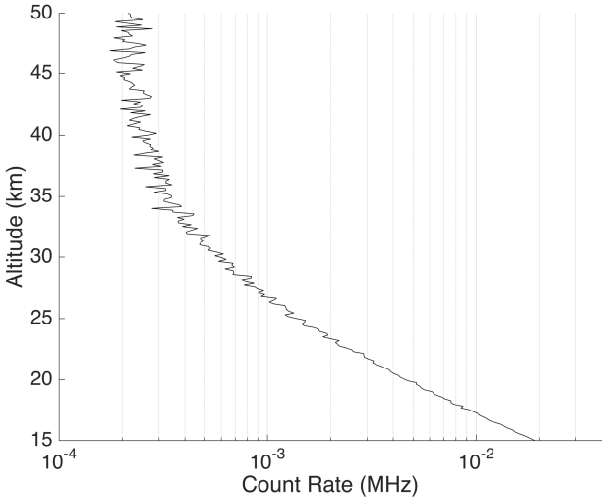

Figure 9. Return signal for RALMO lidar for the night of 23 April 2013, from 1:16 to 5:30 am.

signal is shown in Fig. 9, for the clear night of 23 April 2013. RALMO lidar uses 3.75 m range bins, however, in this Figure the range bins are co-added to 150 m as well as co-added in time for the entire night (from 1:16 to 5:30 am local time). At 30 km, the RALMO system photon count rate is only about 0.0005 MHz which for a Rayleigh channel is very low and this value at 20 km is 0.004 MHz. We followed Jalali et al. (2018) for the OEM RALMO Rayleigh temperature retrieval with the following exceptions. The data grid 150 m, the retrieval grid is 300 m and We didn't retrieve the deadtime for the RALMO as it is linear in the retrieval hight ranges. Also, we used the monthly ozone climatology (Steinbrecht et al., 2009) calculated by DWD lidar for the values and standard deviations of the ozone density in the forward model.

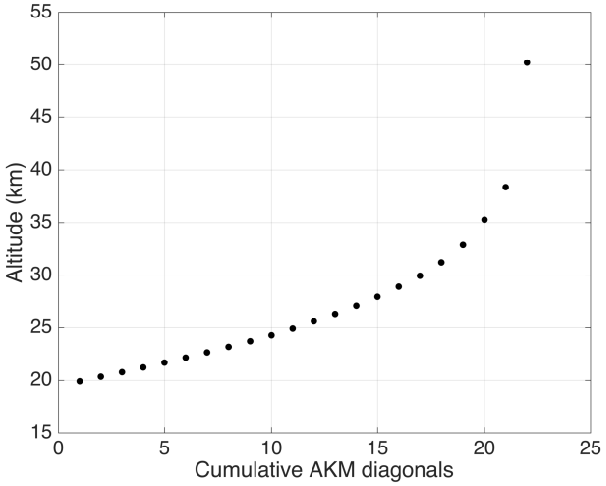

Figure 10. The coarse grid altitude.

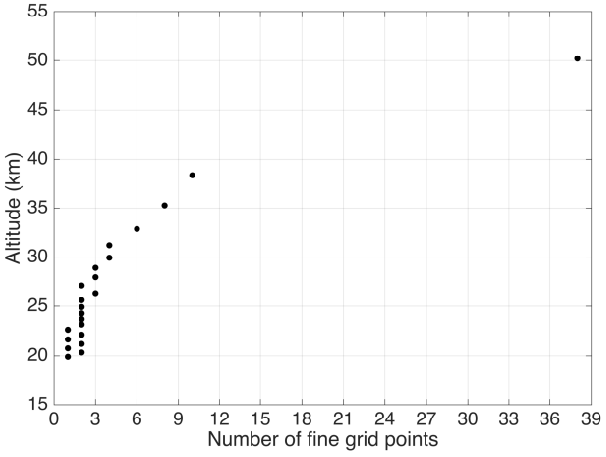

Figure 11. The number of fine grid points used to calculate the coarse grid.

Fig. 12 shows the averaging kernel matrices for the fine and coarse grid. The measurement response in the fine grid even in lower altitudes is not 1, which indicated of contribution of *a priori* in the retrieval.

The statistical uncertainty follows the Poisson distribution and lidar statistical uncertainty proportional to the inverse of square root of photon count. The RALMO photon count is small and therefore, its statistical uncertainty is large (Fig. 13). The RALMO statistical uncertainty in the fine grid is around 4 K at 20 km which this value increase rapidly and reaches to 8 K at 30 km and 11 k at 40 km. These values are larger on the coarse grid, 7 K at 20 km, 11 K at 30 km and 40 k at 40 km. The statistical uncertainties presented in Fig. 13 are several order smaller than the statistical uncertainty. The pattern of the statistical uncertainties is same as the PCL, which they increase with height on the coarse grid as the retrieval grid increases.

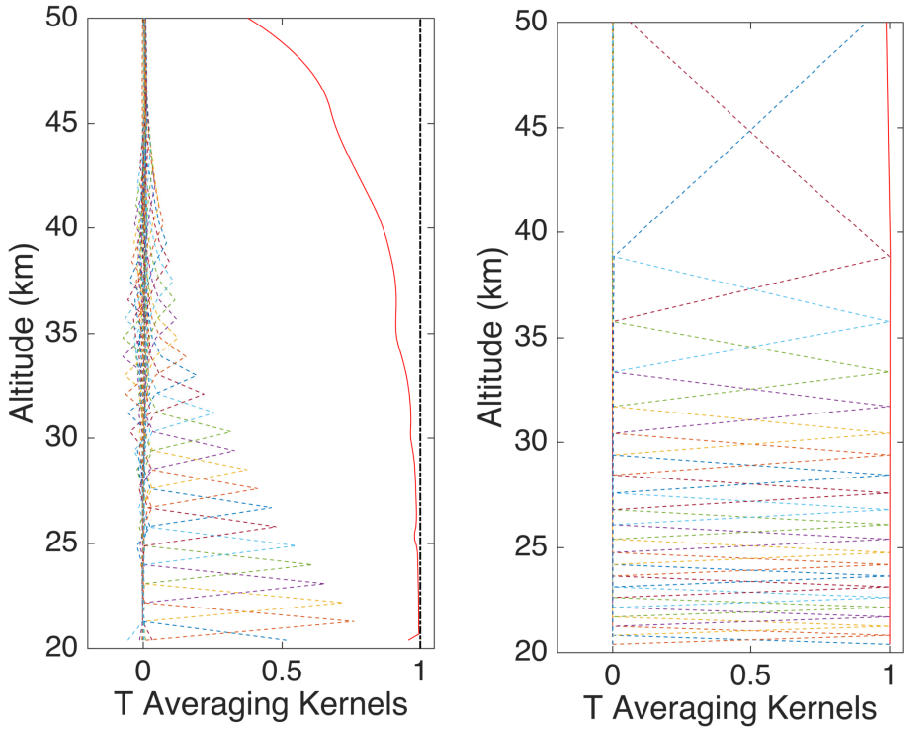

Figure 12. The averaging kernel matrix on the fine grid (left) and on the coarse grid (right).

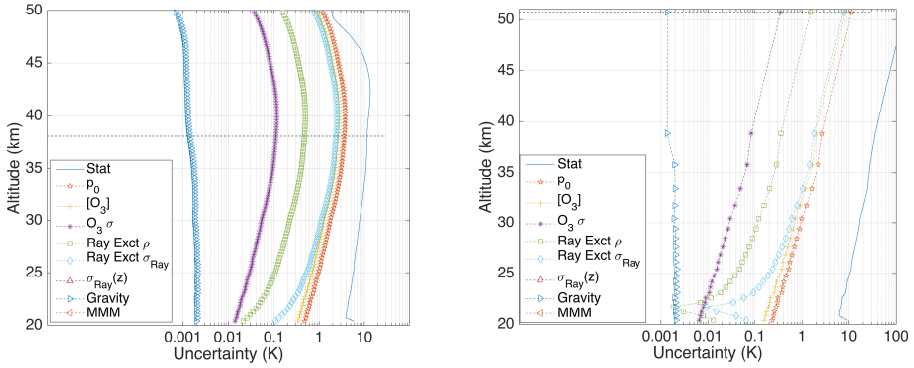

Figure 13. Total uncertainty budget on the fine (left) and coarse (right) grid.

8.3 Nighttime RALMO water vapour *a priori* removal

We have applied the *a priori* removal method to one nighttime and one daytime OEM water vapour retrieval using the RALMO lidar. The nighttime retrieval uses a 30 minute integration on April 23rd, 2014 from 22:00 to 22:30 at the time of the radiosonde launch. This is the same night used in the RALMO Rayleigh temperature retrieval discussed above, although at an earlier time in order to compare with the radiosonde. The fine grid for the RALMO water vapour retrieval is 50 m. The coarse grid for the

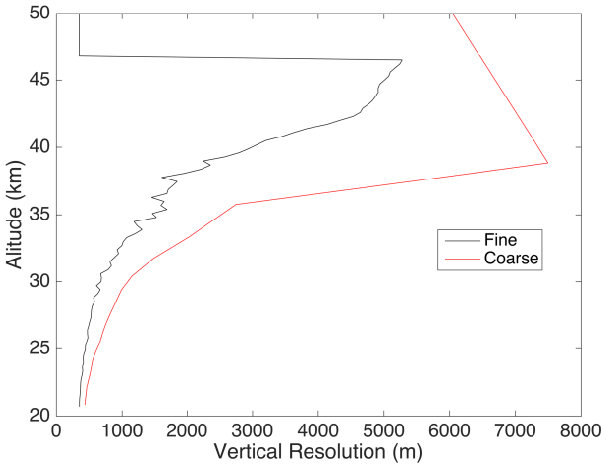

Figure 14. The vertical resolution.

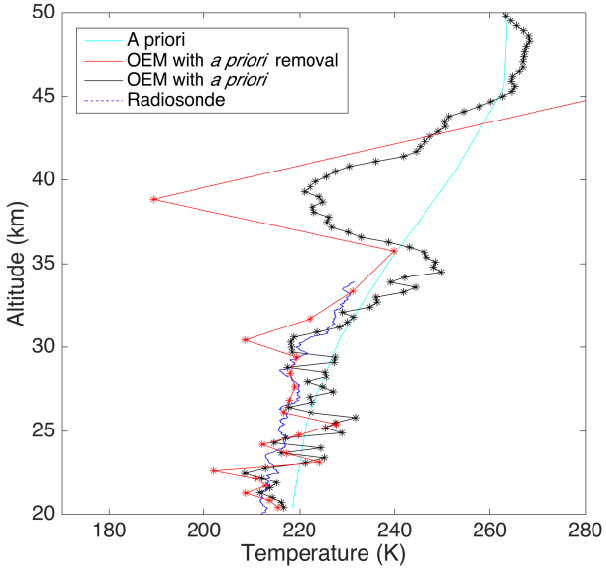

Figure 15. The retrieved temperature.

nightly RALMO water vapour retrieval is shown in Fig. 17 and the average coarse grid resolution above 5 km is 100 m which gradually increases up to 400 m around 11 km (Fig. 18).

The averaging kernel matrix for the fine and coarse grid retrievals are shown in Fig. 19. The 0.9 cutoff for the fine grid retrieval is around 8.5 km, which is typical for the 30 minute night time retrievals. The coarse grid averaging kernels all equal 1, with the second to last altitude at 11 km. Therefore, the method increases the last valid altitude by 2 km.

The vertical resolution between the fine and coarse grid retrievals are the same up to 5 km where they begin to diverge (Fig. 20). The signal at 5 km is small in the water vapour channel above that altitude, therefore the width of the averaging

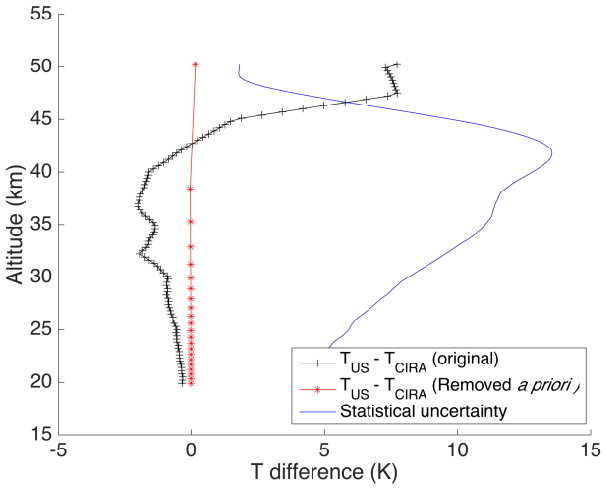

Figure 16. Temperature difference between the OEM retrieved temperature profiles using US Standard Atmosphere and CIRA-86 as the*a priori*.

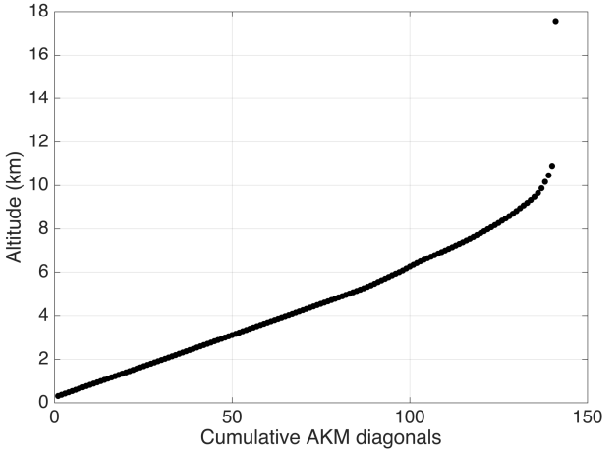

Figure 17. The coarse grid altitude.

kernel increases and more altitudes are needed in the coarse grid. The last point in the vertical resolution is not shown here because it is 6 km and we would not be able to see the rest of the figure. Fig. 21 shows the final water vapour retrievals on the fine and coarse grid, as well as a Vaisala RS92 radiosonde profile for comparison. Both profiles agree past the 0.9 cutoff and up to 9 km at which point the coarse grid retrieval diverges from both the fine grid retrieval and the radiosonde. However, the last two points of the coarse grid retrieval follow the radiosonde measurements. The differences with respect to the radiosonde could be due to the lack of co-location of the instruments since the radiosonde could be several kilometres away from the lidar at that altitude and may not be measuring the same features.

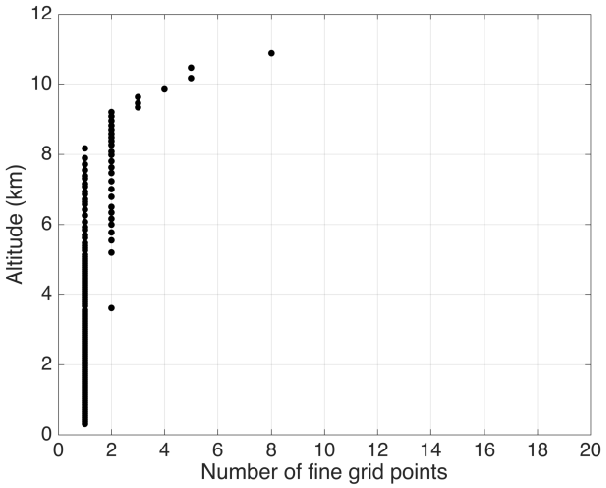

Figure 18. The number of fine grid points used to calculate the coarse grid.

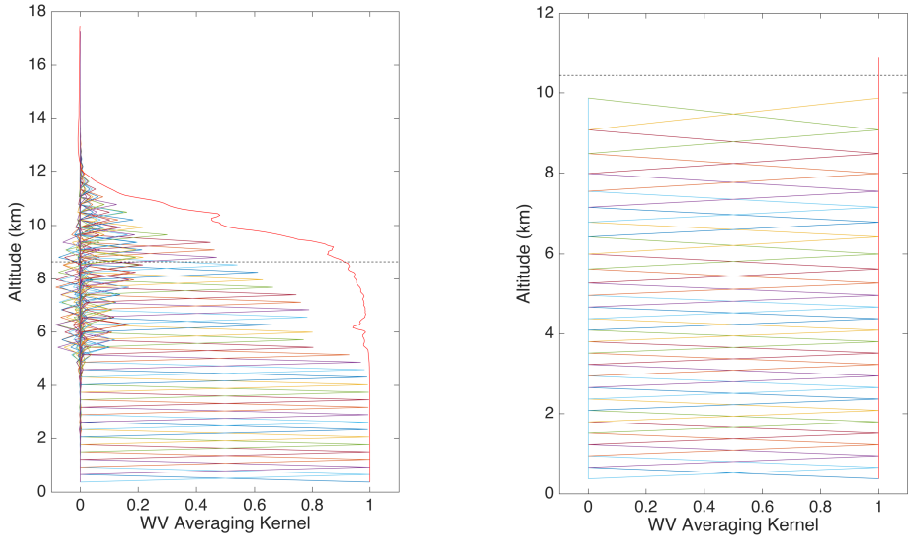

Figure 19. The averaging kernel matrix on the fine grid (left) and on the coarse grid (right).

8.4 Daytime RALMO water vapour *a priori* removal

The signal to noise ratio is much smaller in the water vapour and nitrogen channels during the day, therefore, the OEM profiles are cut off at very low altitudes. We chose one clear daytime water vapour retrieval to investigate the usefulness of the *a priori* method for low signal to noise ratios. The example retrieval is a 30 minute integration on January 22nd, 2013 from 10:00 to 10:30 local time in conjunction with the Vaisala RS92 GRUAN radiosonde launch. Similarly to the nighttime retrieval, the fine grid is 50 m. The estimate of the number of fine grid points used in the coarse grid is shown in Fig. 23 where below 2 km the

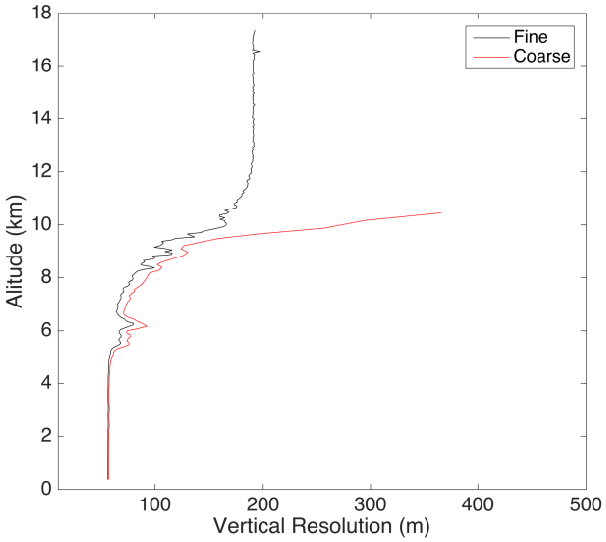

Figure 20. The vertical resolution.

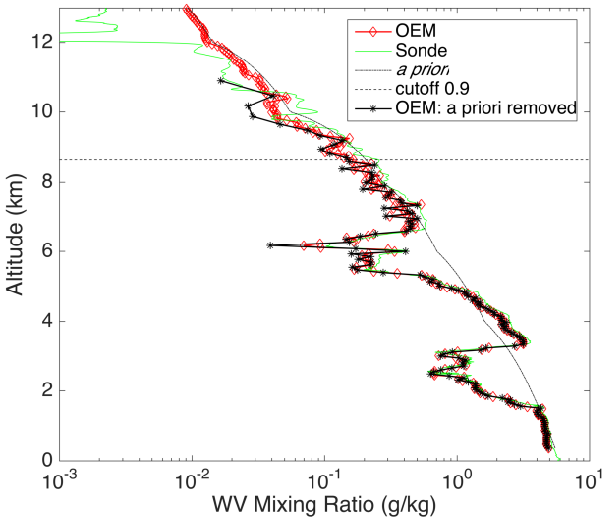

Figure 21. The water vapour retrieval.

majority of points are the same as those on the fine grid. Above 2 km the average resolution is 150 m with second to last point at 7.5 km resolution. The final coarse grid points are shown in Fig. 22.

The daytime averaging kernels are much smaller than the nighttime kernels. The 0.9 cutoff is at 2 km, but does not decrease as rapidly as the nighttime kernels. The coarse grid averaging kernels significantly extend the retrieval range up to 4.5 km.

The daytime water vapour retrievals are shown in Fig. 26. The fine and coarse grid retrievals are the same up to 2.5 km, at which point the coarse grid retrieval begins to follow the path of the radiosonde, and not the fine grid retrieval. The coarse grid

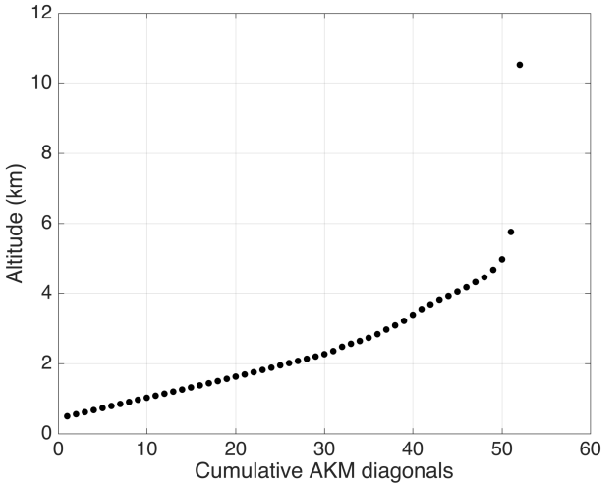

Figure 22. The coarse grid altitude.

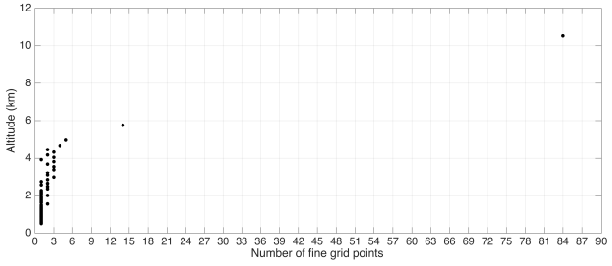

Figure 23. The number of fine grid points used to calculate the coarse grid.

retrieval agrees with the radiosonde until 4.8 km, at which point the vertical resolution is 500 m. Therefore, the last three points in the coarse grid retrieval will not produce results similar to the radiosonde. If we consider the last valid point to be 4.5 km, the *a priori* removal method still significantly extends the valid altitude range of the daytime OEM retrievals by 2.5 km.

9 Summary

10 Discussion

The question that always arises here is what is the effect of the a priori on the temperature retrieval. We have tried to answer this question by showing this distribution of the a priori effect on the temperature climatology from Jalali et al. (2018)(Fig. **??**). Figure **??** shows that 90% of the nights had less than a 5 K influence from the *a priori* temperature profiles. Additionally, in all cases the *a priori* temperature influence were less than the statistical uncertainty, as was illustrated in Figure FIND FIGURE in Jalali et al. (2018).

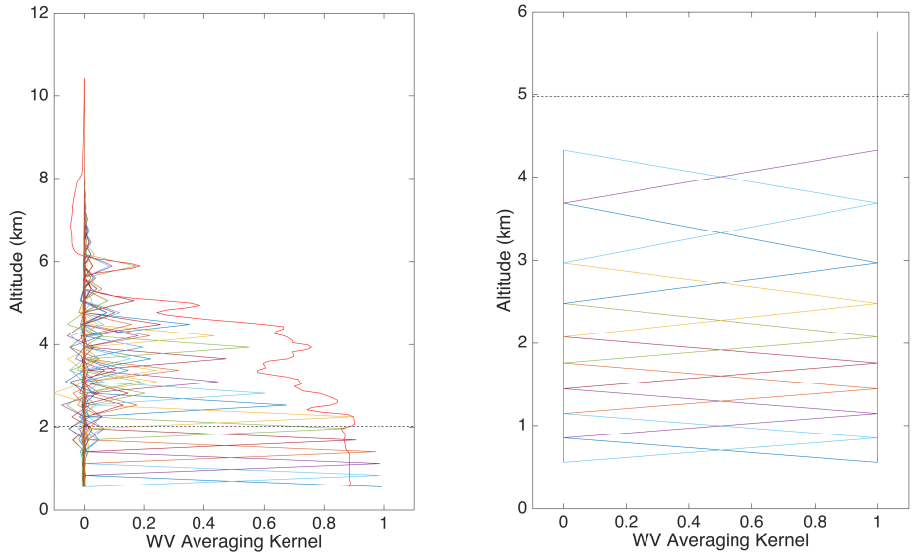

Figure 24. The averaging kernel matrix on the fine grid (left) and on the coarse grid (right).

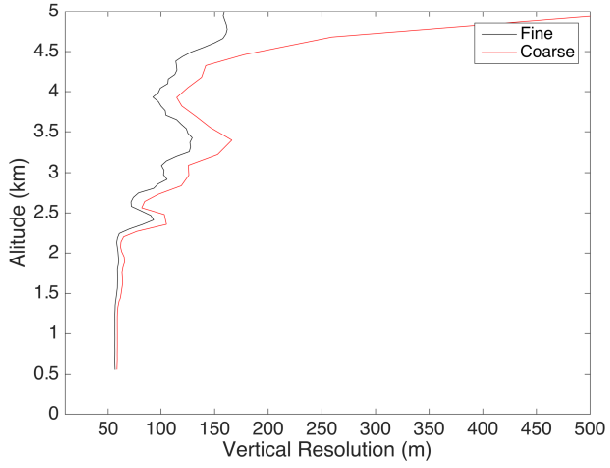

Figure 25. The vertical resolution.

We show how the *a priori* removal method works in four sample retrievals: two Rayleigh temperatures, water vapour night-time, and water vapour daytime. For Rayleigh temperature retrievals we picked measurements from two different lidars to illustrate a high signal-to-noise ratio (SNR) example (PCL) and a low SNR example (RALMO). In RALMO's case, we see more influence from the *a priori* due to its low SNR. RALMO's low signal causes more of an *a priori* contribution in the retrieval. After the *a priori* is removed, the temperature falls back to the true temperature as measured by the Payerne daily C34 radiosonde. In PCL's case the count rates are 1000 times higher than RALMO's at 30 km which results in less of an *a priori* contribution throughout the profile. We compared PCL's temperature to the SABER temperature retrieval on the same

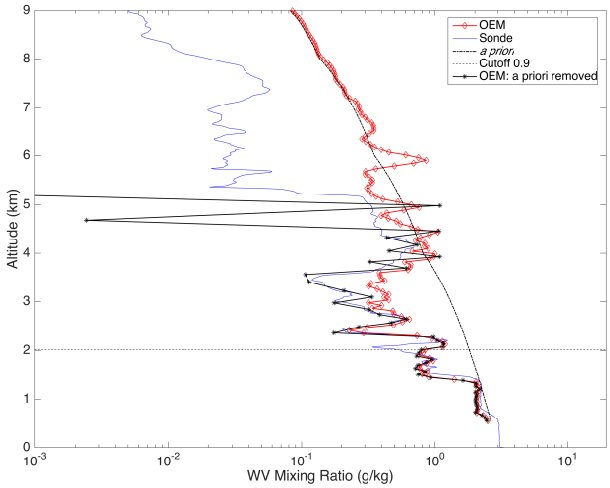

Figure 26. The retrieved temperature.

night, and while they both seem to see the same feature above 90 km they disagree on the altitudes. This is possibly due to the difference in geographical locations - the closest SABER measurements for that night were within 5 degrees of latitude and 24 degrees in longitude from PCL. Another possible reason for the offset could be due to the difference in altitude resolution between the two instruments. In Jalali et al. (2018) it was suggested that the 0.9 level was used as the valid cut-off height. In RALMO and PCL's case we see that the second to last point is very close to the same height, therefore, the 0.9 measurement response value seems to be a valid cutoff.

Water Vapour daytime and nighttime

An advantage of this method is that one can consider the entire profile valid, however, due to the high vertical resolution it does not make sense to include the last point, and in some cases the second-to-last point as well depending on its vertical resolution. This method allows the researcher to analyze the extent to which the OEM retrieval uses the *a priori*. In the regions where the SNR is low or the averaging kernel is less than 1, the *a priori* removal method improves the validity of the retrieval. The systematic uncertainties in the retrieval decreases due to the removal of the inverse of the *a priori* covariance matrix from the gain equation (Eq. 4). However, the statistical uncertainty in the retrieval increases. While the *a priori* removal gives us more confidence in the retrieval, we lose vertical resolution as a consequence.

Author contributions.

Acknowledgements.

References

Ceccherini, S., Raspollini, P., and Carli, B.: Optimal use of the information provided by indirect measurements of atmospheric vertical profiles, Opt. Express, 17, 4944–4958, 2009.

Jalali, A., Sica, R. J., and Haefele, A.: A middle latitude Rayleigh-scatter lidar temperature climatology determined using an optimal estimation method, Atmospheric Measurement Techniques Discussions, 2018, 2018.

Joiner, J. and Silva, A. D.: Efficient methods to assimilate remotely sensed data based on information content, Q. J. Roy. Meteor. Soc., 124, 1669–1694, 1998.

Rodgers, C. D.: Inverse Methods for Atmospheric Sounding: Theory and Practice, vol. 2, World Scientific, Hackensack, NJ, USA, 2011.

Sica, R. J. and Haefele, A.: Retrieval of temperature from a multiple-channel Rayleigh-scatter lidar using an optimal estimation method, Appl. Optics, 54, 1872–1889, 2015.

Sica, R. J. and Haefele, A.: Retrieval of water vapor mixing ratio from a multiple channel Raman-scatter lidar using an optimal estimation method, Appl. Optics, 55, 763–777, 2016.

Steinbrecht, W., Claude, H., Schonenborn, F., McDermid, I. S., Leblanc, T., Godin-Beekmann, S., Keckhut, P., Hauchecorne, A., Gijsel, J. A. E. V., Swart, D. P. J., Bodeker, G. E., Parrish, A., Boyd, I. S., Kampfer, N., Hocke, K., Stolarski, R. S., Frith, S. M., Thomason, L. W., Remsberg, E. E., Savigny, C. V., Rozanov, A., and Burrows, J. P.: Ozone and temperature trends in the upper stratosphere at five stations of the Network for the Detection of Atmospheric Composition Change, International Journal of Remote Sensing, 30, 3875–3886, 2009.

Vincent, R. A., Dudhia, A., and Ventress, L. J.: Vertical level selection for temperature and trace gas profile retrievals using IASI, Atmos. CMeas. Tech., 8, 2359–2369, 2015.

von Clarmann, T. and Grabowski, U.: Elimination of hidden a priori information from remotely sensed profile data, Atmos. Chem. Phys., 7, 397–408, 2007.